

Charge Transport in Pure and Mixed Phases in Organic Solar Cells

Armantas Melianas,* Vytenis Pranculis, Donato Spoltore, Johannes Benduhn, Olle Inganäs, Vidmantas Gulbinas, Koen Vandewal, and Martijn Kemerink*

In organic solar cells continuous donor and acceptor networks are considered necessary for charge extraction, whereas discontinuous neat phases and molecularly mixed donor–acceptor phases are generally regarded as detrimental. However, the impact of different levels of domain continuity, purity, and donor–acceptor mixing on charge transport remains only semi-quantitatively described. Here, cosublimed donor–acceptor mixtures, where the distance between the donor sites is varied in a controlled manner from homogeneously diluted donor sites to a continuous donor network are studied. Using transient measurements, spanning from sub-picoseconds to microseconds photogenerated charge motion is measured in complete photovoltaic devices, to show that even highly diluted donor sites (5.7%–10% molar) in a buckminsterfullerene matrix enable hole transport. Hopping between isolated donor sites can occur by long-range hole tunneling through several buckminsterfullerene molecules, over distances of up to ≈ 4 nm. Hence, these results question the relevance of “pristine” phases and whether a continuous interpenetrating donor–acceptor network is the ideal morphology for charge transport.

mixture of electron donating and accepting materials—a bulk heterojunction (BHJ). Such interpenetrating donor–acceptor mixtures form complicated multilength scale morphologies, often involving several phases such as ordered/disordered donor, mixed donor–acceptor and ordered/disordered acceptor. The coexistence of neat and mixed donor–acceptor domains is thought to be beneficial as it could provide an energy cascade^[4,5] for charge separation,^[6,7] followed by charge transport in the neat phases. However, the neat regions may be discontinuous, forcing charges to cross mixed domains multiple times during extraction. If the mixed regions are severely disordered or contain less than the percolation threshold of required material, charge transport is thought to deteriorate significantly, limiting device performance.^[8]

1. Introduction

Organic photovoltaics (OPV) allows for a low-cost alternative to inorganic solar cells, with recent developments showing power conversion efficiencies of 10%–12%.^[1–3] The photoactive layer in an OPV device is most commonly based on a disordered

The effect of donor–acceptor mixing (or phase purity) on charge transport has been previously addressed using microstructural characterization,^[9,10] steady-state,^[11–13] and/or time-resolved^[14–16] mobility measurements on BHJs with a varying donor–acceptor stoichiometry and/or processing conditions. Although such studies have revealed important trends, they remain mostly semiquantitative—the question of how pure the neat domains have to be and how detrimental domain discontinuities or donor–acceptor mixing are in relation to charge transport kinetics remains to a large extent unanswered. Not knowing which important charge transport features to optimize, limits the development of next generations of organic optoelectronic devices.


Here, we address this by measuring photo-generated charge motion from the first hopping events (with sub-picosecond time resolution) to full extraction in complete solar cell devices based on coevaporated bulk heterojunctions of α -sexithiophene (α -6T) and buckminsterfullerene (C_{60}). We carefully vary the molar fraction of α -6T in C_{60} from homogeneously diluted (<10% molar), to a point where α -6T begins to form isolated aggregates (>10%–25% molar) or is strongly aggregated (50% molar). We thus vary the distance between isolated α -6T sites and the level of disruption of the C_{60} phase in a controlled manner—the α -6T: C_{60} system may be viewed as a model for the mixed donor–acceptor phase in OPV. C_{60} was chosen as the model acceptor since its use in organic electronics is

Dr. A. Melianas, Prof. O. Inganäs, Prof. M. Kemerink
Department of Physics, Chemistry and Biology
Linköping University
Linköping 58183, Sweden
E-mail: Armantas.Melianas@liu.se; Martijn.Kemerink@liu.se

V. Pranculis, Prof. V. Gulbinas
Center for Physical Sciences and Technology
Saulėtekio av. 3, Vilnius LT-10257, Lithuania

Dr. D. Spoltore, J. Benduhn, Prof. K. Vandewal
Dresden Integrated Center for Applied Physics and Photonic Materials
(IAPP) and Institute for Applied Physics
Technische Universität Dresden
Dresden 01062, Germany

Prof. V. Gulbinas
Department of General Physics and Spectroscopy, Faculty of Physics
Vilnius University
Saulėtekio 9, Vilnius LT-10222, Lithuania

 The ORCID identification number(s) for the author(s) of this article can be found under <https://doi.org/10.1002/aenm.201700888>.

DOI: 10.1002/aenm.201700888

ubiquitous, whereas α -6T was picked as the model donor as it consists of a sequence of thiophene units, similar to many conjugated donors, e.g., poly(3-hexylthiophene) (P3HT). The well-defined sample morphology and the unique time resolution of our transient measurements enables us to quantify the impact of donor–acceptor mixing on the charge transport kinetics.

We experimentally show that even when the donor sites are highly diluted (5.7%–10% molar) and the donor phase is discontinuous, hole transport between isolated donor sites nevertheless occurs by long-range hole tunneling through several buckminsterfullerene molecules (over distances of up to ≈ 4 nm)—an often overlooked hole transport mechanism in organic solar cells. We demonstrate that for conditions relevant to OPV device operation, hole transport between isolated donor sites occurs with a reasonably high hole mobility ($\mu_h = 5\text{--}15 \times 10^{-5} \text{ cm}^2 \text{ V}^{-1} \text{ s}^{-1}$, depending on the concentration of the donor). We find that at low amounts of the donor (<10% molar) electron transport in the C_{60} phase remains unperturbed ($\mu_e = 2 \text{ cm}^2 \text{ V}^{-1} \text{ s}^{-1}$), so the C_{60} phase may be considered as effectively pure for electron transport. As such, C_{60} domains containing only a trace amount of donor enable ambipolar transport by long-range hole tunneling. This shows that the general notion that a continuous donor network is strictly necessary for hole transport is incorrect.

Furthermore, we demonstrate that at high reverse bias and low donor concentration (1.5%–25% molar) a small fraction of the hole population (0%–20% of the total, depending on bias) can be transferred to and extracted via C_{60} with a high hole mobility ($\mu_h = 0.1\text{--}2 \text{ cm}^2 \text{ V}^{-1} \text{ s}^{-1}$ for 25%–1.5% donor in C_{60}). Nevertheless, for conditions relevant to OPV device operation, facile hole capture by isolated donor sites rapidly reduces the fraction of holes transported in C_{60} to zero, in which case subsequent hole motion occurs by long-range tunneling between isolated donor sites.

2. Results

2.1. α -6T: C_{60} as a Model System for the Mixed Phase

We study coevaporated bulk heterojunctions of α -6T and the neat fullerene C_{60} as a model system for the mixed donor–acceptor phase in OPV. Controlled evaporation under ultrahigh vacuum allows us to precisely vary the molar fraction of α -6T in C_{60} , and thereby tune the distance between isolated α -6T (see Table S1 in the Supporting Information) and the degree of donor–acceptor mixing (Figure 1a). This is in contrast to solution-cast polymer OPV blends, where the interdonor-site distance is very challenging, if not impossible, to tune reliably: the polymer chain enforces at least one additional length scale, since it has at least one typical intra-chain and at least one typical inter-chain distance.

It was first shown by Tang et al.^[17] and later repeated by others,^[18] that even low donor amounts in a C_{60} matrix (5% by weight) lead to OPV devices with a peak external quantum efficiency (EQE) $\approx 70\%$ for various small molecule donors. Using C_{70} peak EQE $\approx 75\%$ – 80% .^[17,19,20] For the α -6T: C_{60} series we also obtain a peak EQE = 70% and fill factor (FF) = 0.55–0.57 at α -6T content in the range of 4%–7% by weight (5.7%–10% molar)

with similar device characteristics as reported by Tang et al., Figure S1 and Table S2 (Supporting Information). As such, the results that are presented here are expected to be general and applicable to other small-molecule-donor and neat fullerene (C_{60} or C_{70}) mixtures.

Since α -6T has a strong tendency to aggregate, it enables us to accurately identify the transition from diluted and largely unaggregated α -6T to the aggregated α -6T phase by analysis of spectroscopic data shown below. The relatively weak absorption coefficient of α -6T compared to that of C_{60} also enables us to simultaneously record spectral blueshifts of the C_{60} phase—a measure for the increased disorder of C_{60} .^[21]

Figure 1b shows EQE measurements that enable us to characterize the morphology of the active layer. The spectra are normalized to the C_{60} absorption peak at 2 eV, corresponding to an intramolecular singlet absorption of C_{60} ,^[21] and scaled by the molar fraction of C_{60} . As C_{60} is the main absorber in these blends, the EQE spectra above 1.8 eV are mainly dominated by the absorption in C_{60} (optical gap $C_{60} \approx 1.8$ eV, optical gap α -6T ≈ 2.3 eV), whereas below 1.8 eV the spectra are dominated by the absorption of the charge-transfer (CT) state manifold, see Figure S2 (Supporting Information). The CT state absorption strength is proportional to the density of CT states in the blend and is a direct measure of the donor–acceptor interfacial area.^[18] When the donor is homogeneously diluted in C_{60} , the interfacial area is, therefore, expected to scale linearly with the donor content. Up to α -6T content of 10% this is indeed the case, as can be observed when the CT manifold is fitted by a Gaussian distribution according to Marcus theory,^[22] see inset of Figure 1b. We observe a deviation from the linear trend at a donor content of 25% indicative of the onset of α -6T aggregation. Donor aggregation is clearly visible only when the donor fraction is 50%, with a strongly redshifted CT absorption.

X-ray reflectivity (XRR) measurements at high donor content ($\approx 25\%$ – 50% molar) indicate pure α -6T aggregates, whereas grazing-incidence X-ray diffraction (GIXD) shows smeared out diffraction peaks, indicating randomly oriented α -6T aggregates with no preferred orientation.^[23] Therefore, up to a donor content of 10% molar, α -6T is homogeneously diluted at random orientations in C_{60} . At higher donor content (10%–25% molar) a mixture of mostly isolated α -6T and some randomly oriented and isolated α -6T aggregates occurs. We will show below that up to α -6T content of 50%, when a large fraction of α -6T aggregates is expected, the donor phase remains discontinuous. As such, we vary the distance between isolated α -6T sites and the level of disruption of the C_{60} phase in a controlled manner, from a purely diluted donor to a discontinuous donor network with aggregates—a model system to study the effects of donor–acceptor mixing on the charge transport kinetics.

2.2. Time-Resolved Charge Extraction

To quantify how the purity of the neat phases affects photogenerated charge transport, we have followed their motion from photogeneration to full extraction in complete solar cell devices. We rely on a combination of the time-resolved electric-field-induced second harmonic generation (TREFISH) technique^[24] combined with photocurrent measurements,^[25] enabling us to

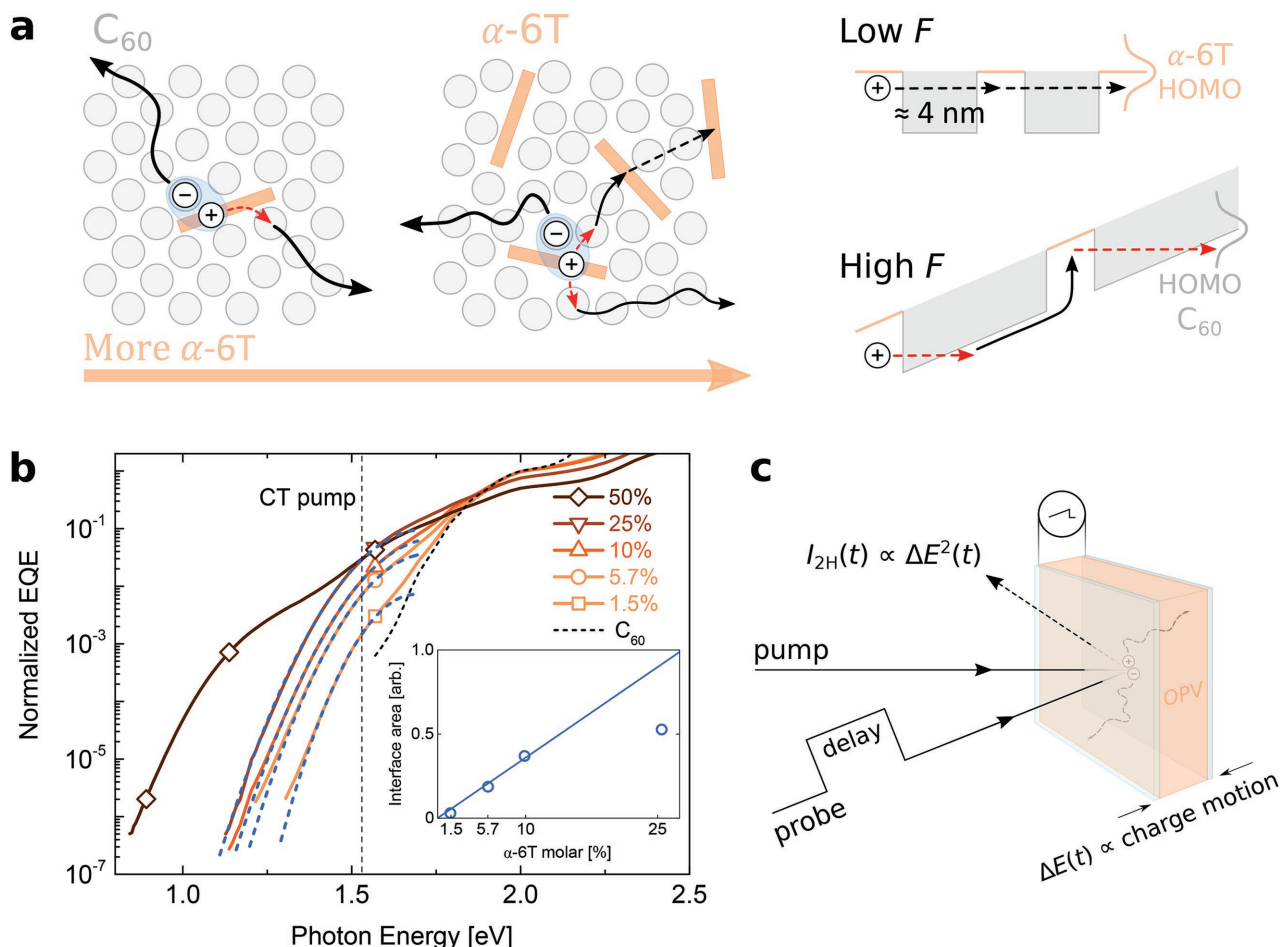


Figure 1. Schematic representation of charge transport in the investigated OPV devices, their EQE spectra and a scheme of the transient measurement technique. a) With increasing donor content the distance between isolated α -6T decreases but the C_{60} matrix gets increasingly disordered. Electron or hole transport in C_{60} is indicated by solid black arrows. Dashed red arrows indicate hole detrapping from α -6T to C_{60} by Fowler–Nordheim-type tunneling (only occurs at high electric fields F), whereas black dashed arrows indicate long-range hole tunneling through C_{60} to nearby α -6T sites. Sites are spread according to a Gaussian DOS distribution as indicated. b) Sensitive EQE measurements. The inset shows the strength of CT absorption as inferred from Gaussian fitting to the CT state manifold (dashed blue traces), see the main text. c) Schematic description of the combined TREFISH and photocurrent experiment.

follow the motion of photogenerated carriers from the first hopping events, occurring on a sub-picosecond to picosecond time scale after photoexcitation, to full extraction.

Figure 1c shows the measurement scheme. The motion of photogenerated charges partially screens the electric field E induced by the applied bias, resulting in a change $\Delta E(t)$. The resulting change $\Delta E(t)$ is detected optically by a measurement of the second-harmonic intensity $I_{2H}(t) \propto \Delta E^2(t)$, enabling sub-picosecond temporal resolution. The TREFISH measurement is complemented by a simultaneous (using the same pump pulse) recording of the photocurrent transient using an oscilloscope. As such, all relevant time scales for charge transport, from sub-picoseconds to tens of microseconds, are probed in a single measurement.

In our time-resolved measurements we have deliberately chosen low energy pump photons (1.53 eV) to only excite the CT state manifold, as indicated by the black dashed line in Figure 1b. At 1.53 eV we are predominantly exciting the

(isolated α -6T): C_{60} interfaces and not those of (aggregated α -6T): C_{60} , as the absorption of the latter occurs at lower photon energies (Figure 1b). Figure S2 (Supporting Information) shows that at 1.53 eV photogeneration in the C_{60} phase can be neglected for all donor concentrations. This ensures that the starting point of the time-resolved measurement is an excited CT complex at the (isolated α -6T): C_{60} interface, instantaneously creating an electron in C_{60} and a hole in isolated α -6T.

Figure 2 shows the time-resolved extraction of photogenerated charges from OPV devices with an increasing molar fraction of α -6T at the indicated applied reverse bias U , where $U = -0.1$ V corresponds to (close to) short-circuit conditions ($U = 0$ V was not possible for technical reasons, see the Experimental Section). We have previously experimentally demonstrated that these traces represent the cumulative amount of photogenerated charge collected at the electrodes.^[25,26]

Before we proceed with the detailed analysis of these kinetics, we highlight that these measurements were performed

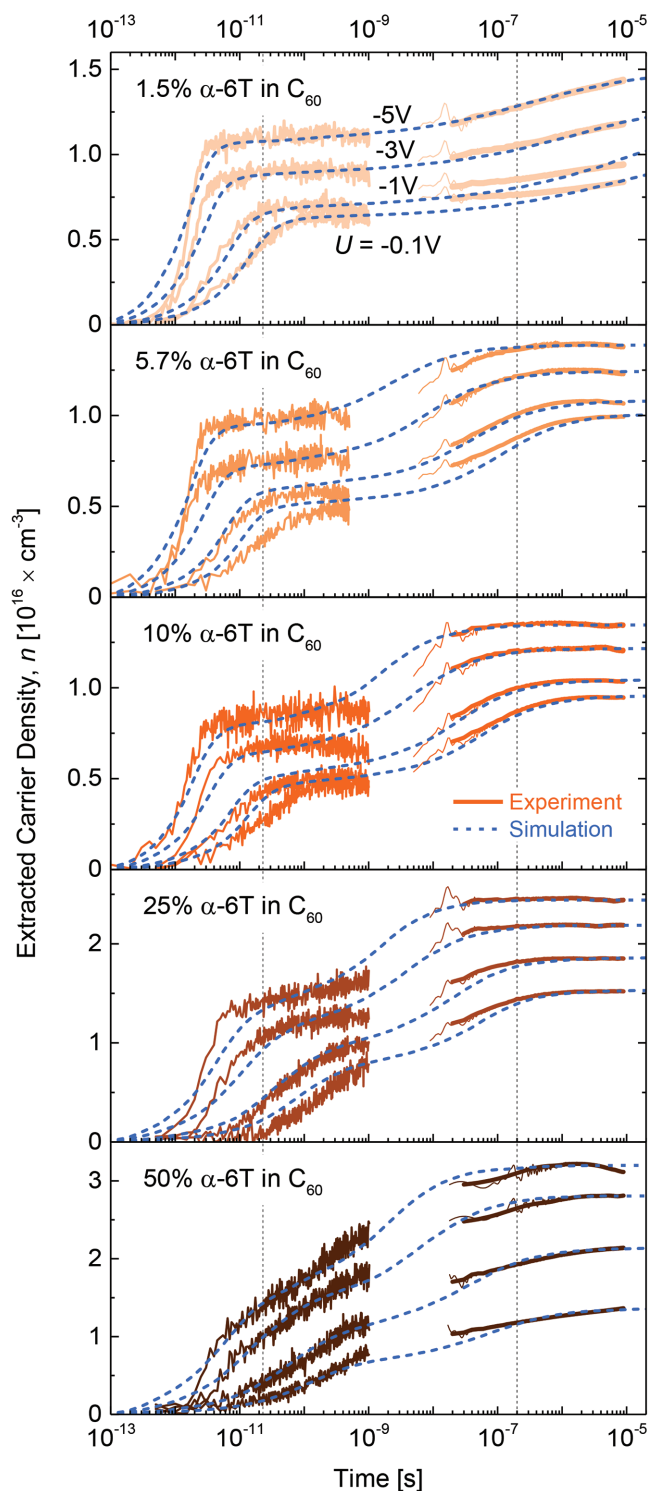


Figure 2. Time-resolved extraction of photogenerated charges. Experiments (colored traces) at the indicated applied reverse bias U and least-square fits by the extended Gaussian disorder model (blue dashed traces) involving three charge carrier populations: electrons in C_{60} , holes in C_{60} and holes tunneling through C_{60} between isolated α -6T sites. Increasing orange color saturation indicates increasing α -6T molar fraction (from top to bottom).

at relatively low excitation fluences (see the Experimental Section), leading to extracted carrier densities n comparable to those found in typical well-performing OPV devices under steady-state AM1.5 illumination (of the order of $n = 10^{16} \text{ cm}^{-3}$, as in Figure 2).^[27–29] To confirm that the extraction kinetics of Figure 2 do indeed describe the charge transport physics of operating OPV devices, we first directly compare our transients to steady-state current–voltage (IV) measurements on the same device.

Figure 3a shows good agreement between steady-state photocurrent–voltage measurements under AM1.5 illumination (blue trace, 10% α -6T device, Figure S3 in the Supporting Information shows other devices) and photocurrent– V curves reconstructed using the transient measurements (solid orange traces). The steady-state photocurrent– V data were obtained by subtracting the steady-state IV measurements in the dark from IV s under illumination. The photocurrent versus V curves from transient measurements were estimated by recording the total amount of collected charge at $t = 10 \mu\text{s}$ versus applied bias and were scaled to match at $U = -5 \text{ V}$ for comparison. This is allowed because transient measurements were performed in the linear pump-fluence regime, see Figure S4 (Supporting Information). We obtain a similarly good agreement when using only a continuous 785 nm laser (1.58 eV) (Figure 3a blue symbols), see Figure S3 in the Supporting Information for agreement in other devices. This confirms that the transient data in Figure 2 represents the conditions relevant for steady-state device operation and thus reflects charge extraction/recombination as they occur in operating OPV devices under AM1.5 illumination.

2.3. Long-Range Hole Tunneling

When α -6T is homogeneously diluted, it is not evident how the holes photogenerated in the CT state are extracted from the OPV device. We demonstrate below that a small fraction (0%–20%, depending on bias) of photogenerated holes is transferred to and extracted via C_{60} , whereas the remaining majority of the holes (80%–100%) is transported between isolated donor sites by long-range hole tunneling through C_{60} .

Transient data in Figure 2 indicate two extraction plateaus, most clearly visible for the 5.7% and 10% devices. Given the approximate temporal position of these extraction plateaus $t = 2.3 \times 10^{-11} \text{ s}$ and $t = 2 \times 10^{-7} \text{ s}$ (black dashed lines in Figure 2), charge carrier mobilities of $\mu = 0.5 \text{ cm}^2 \text{ V}^{-1} \text{ s}^{-1}$ and $\mu = 6 \times 10^{-5} \text{ cm}^2 \text{ V}^{-1} \text{ s}^{-1}$, respectively, are expected. The latter part of the transients is attributed to hole motion via isolated α -6T sites, as confirmed by steady-state hole-only mobility measurements using space-charge limited currents (SCLC) giving $\mu_h = 6 \times 10^{-5} \text{ cm}^2 \text{ V}^{-1} \text{ s}^{-1}$ (at 10% molar), see Figure S5 (Supporting Information). On basis of the high electron mobility reported in neat C_{60} crystals ($\mu_e = 0.5 \text{ cm}^2 \text{ V}^{-1} \text{ s}^{-1}$),^[30] we attribute the early part of the transients mainly to the extraction of electrons. However, as we will show below, a small fraction of holes (0%–20%, depending on bias) is also extracted very rapidly via C_{60} .

As photogenerated carriers are generated in pairs the amount of extracted holes should be equal to that of electrons.

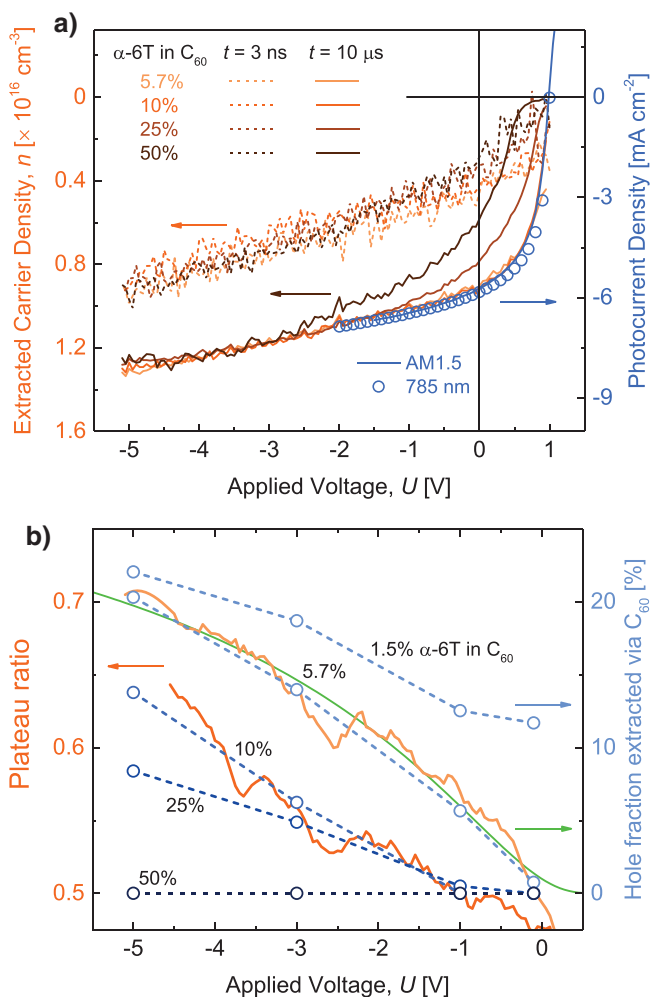


Figure 3. Photocurrent–voltage characteristics and the fraction of photo-generated holes extracted via C_{60} . a) Steady-state photocurrent–voltage measurements under AM1.5 illumination (blue trace, corrected by the dark IV, 10% α -6T device, Figure S3 in the Supporting Information shows other devices), steady-state photocurrent–voltage measurements under continuous 785 nm laser illumination (blue symbols, corrected by the dark IV, scaled to AM1.5 data, scaling factors shown in Figure S3 in the Supporting Information) and the total collected charge recorded by pulsed measurements (solid orange traces $t = 10 \mu\text{s}$). Dashed orange traces indicate the total photogenerated charge extracted at $t = 3 \text{ ns}$. b) Orange traces indicate the experimental plateau ratio in extracted carrier density for the 5.7% and 10% α -6T devices in Figure 2. Higher ratios than 0.5 indicate that a fraction of holes is extracted via C_{60} (right axis). Blue traces are the estimated hole fraction from the model fits to experiment in Figure 2. The green trace is a fit to Fowler–Nordheim-type tunneling.^[32]

This is clearly visible for 5.7% and 10% devices at (close to) short-circuit conditions ($U = -0.1 \text{ V}$), where the extraction plateau ratio is very close to 0.5 (Figure 3b), whereas it is difficult to discern for the remaining samples and is not shown. A ratio of 0.5 means that the early time plateau is entirely dominated by the fast extraction of electrons and that all holes are extracted via isolated donor sites. However, we observe that with increasing reverse bias the fraction of photogenerated charges extracted at early times is increasing above 50% (Figure 3b),

suggesting that an increasing fraction of holes is extracted very rapidly. Given the high hole mobility reported in neat C_{60} crystals ($\mu_{\text{h}} = 2 \text{ cm}^2 \text{ V}^{-1} \text{ s}^{-1}$)^[30] this suggests that an increasing fraction of holes is extracted via C_{60} , which we will discuss below. Nevertheless, Figure 3b shows that for the fields relevant to OPV devices ($U = 0 \text{ V}$ corresponds to short-circuit conditions), hole trapping reduces the fraction of holes transported in C_{60} to zero, forcing all holes to move via isolated α -6T.

The mechanism for the initial hole transfer to C_{60} at high reverse bias is not entirely clear, as following photoexcitation in the CT manifold, the hole is expected to initially reside in α -6T. Furthermore, based on the difference between the highest occupied molecular orbital (HOMO) levels of α -6T (-5.3 eV) and C_{60} (-6.2 eV), as determined by ultraviolet photoelectron spectroscopy (UPS),^[31] the energetic barrier for hole transfer from α -6T to C_{60} is expected to be roughly $0.9 \text{ eV} = 35 kT$. Hence, thermal detrapping of the hole seems unlikely.

Instead, we propose that hole transfer to C_{60} may be assisted by Fowler–Nordheim-type tunneling through a triangular barrier (Figure 1a), as confirmed by good fits to the Fowler–Nordheim equation,^[32] describing the tunneling probability (green trace in Figure 3b). For the equally good fits at other donor fractions see Figure S6 (Supporting Information). In principle, the tunneling probability of a particle with excess energy (such as after photoexcitation) is higher than that of a particle tunneling from the lowest energy of the trap site (such as after a prolonged trapping event). We speculate that photo-induced hole transfer to C_{60} may occur before on-site thermalization, faster than $\approx 1 \text{ ps}$,^[33] effectively lowering the tunneling barrier (compare the two situations at high field F in Figure 1a). This process divides the extracted hole population into two distinct parts: holes transferred to C_{60} and extracted very rapidly and holes trapped in isolated α -6T and extracted slowly. For a more detailed discussion, see Figures S6 and S7, and Notes S1 and S2 (Supporting Information). Nevertheless, for the practically relevant fields to OPV devices all holes remain trapped in isolated α -6T.

Following spatial trapping in isolated α -6T sites, there are two possible mechanisms for further hole transport. Either the hole escapes α -6T and is transported via C_{60} until a further trapping event, or the hole instead tunnels through C_{60} to another α -6T. On basis of the large energy barrier for thermal hole detrapping from α -6T to C_{60} ($0.9 \text{ eV} = 35 kT$) and the unlikelihood of Fowler–Nordheim-type tunneling at low fields between short-circuit and V_{OC} , both detrapping scenarios seem unlikely. At low fields long-range hole tunneling through several C_{60} molecules to neighboring trap sites seems more plausible. Note that in this case the tunneling mechanism is different as at low fields the barrier is expected to be rectangular (Figure 1a) with a tunneling probability that is independent of field, see Figure S6 and Note S2 (Supporting Information). A similar transition from direct tunneling to field emission at moderate bias ($< 1 \text{ V}$) has been demonstrated by Kushmerick et al. in molecular junctions of π -conjugated thiols.^[34]

The mean center-to-center distance between isolated α -6T decreases from roughly $\approx 5.3 \text{ nm}$ to $\approx 3.4 \text{ nm}$ when going from 1.5% to 5.7% molar α -6T in C_{60} . Table S1 (Supporting Information) shows details on the conversion between weight, molar, and volume fractions, and the deduced distance between

isolated α -6T molecules. The extraction kinetics in Figure 2 clearly indicate that upon going from 1.5% to 5.7% molar α -6T, the second extraction plateau (at microsecond time scales) grows and shifts to significantly shorter times. This suggests that the onset for efficient long-range hole tunneling through C_{60} to neighboring α -6T lies roughly in the 3.4–5.3 nm range (≈ 4 nm), which corresponds to a distance of several C_{60} molecules (C_{60} diameter is 0.71 nm, center-to-center distance is ≈ 1 nm). A similar onset from direct to thermally activated tunneling ≈ 4 nm has been reported by Frisbie et al. in π -conjugated molecular wires.^[35]

Although at low donor fractions (5.7%–10% molar) long-range hole tunneling is already evident from the experimental data alone, at higher donor content (25%–50% molar) the situation is less clear; not only the packing of C_{60} may be significantly distorted, but also the α -6T phase may form a discontinuous network, reducing the fraction of holes that undergo long-range tunneling. At this point an advanced charge transport model is required to quantitatively explain the kinetics.

2.4. Simulations Using the Gaussian Disorder Model

To simulate the extraction of three charge carrier populations—electrons in C_{60} , holes in C_{60} , and holes tunneling through C_{60} between isolated donor sites—we rely on the extended Gaussian Disorder Model (eGDM),^[36] which has been successfully utilized to explain carrier hopping in a large variety of organic semiconductors. Note that although hole tunneling discussed here occurs over larger distances and through C_{60} (as opposed to a barrier of empty space), it can still be described by the same eGDM formalism, see Note S3 (Supporting Information).

In brief, the model^[37] takes into account: electron-hole recombination; all Coulomb interactions; charge transport via a field- and density-dependent carrier mobility, consistent with the parametrization by Pasveer et al.;^[38] charge extraction and injection at contacts. The field-dependence of charge extraction observed in Figure 2 is fitted globally (by a single parameter set), using an iterative least-squares procedure, thus eliminating possible errors due to manual fitting and severely constraining the fit parameters. We have previously shown that our model can successfully fit both transient TREFISH and steady-state SCLC experiments using the same parameter set,^[37] which was also done here, as described in Figure S5 and Table S3 (Supporting Information).

Figure 2 shows that our simulations capture the charge extraction dynamics observed in experiment reasonably well. The applied bias U in simulations was corrected for the built-in field U_{bi} of the OPV device, experimentally determined as the bias at which the extracted charge density in the transient measurement is equal to zero ($U_{bi} = 1$ V in Figure 3a). Model fits allow us to more accurately quantify the fraction of photogenerated holes transported in C_{60} (blue traces in Figure 3b), especially for the 1.5%, 25%, and 50% devices, for which the extraction plateaus are not clearly visible in experiment (Figure 2). In agreement with the earlier observation from transient data, the hole fraction extracted via C_{60} is increasing with reverse bias.

From experimental data alone we cannot distinguish whether the small fraction of holes transferred to C_{60} (Figure 3b) is extracted without a single trapping event or whether multiple trapping/detrapping events occur during hole extraction via C_{60} . To quantify, we have extended our modeling to account for the morphology of the BHJ active layer: a fraction of the total simulated volume $90 \times 90 \times 50$ nm³ was occupied by randomly dispersed α -6T sites, using the known volume fractions. These simulations (Figure S7, Supporting Information) suggest that the fast fraction of holes (0%–20% of the total in Figure 3b) consist of holes extracted via C_{60} without a single trapping event (0%–10% of the total) and holes captured by α -6T but undergoing ultrafast Fowler–Nordheim-type detrapping back to C_{60} (possible only at high fields F). Nevertheless, the majority of the holes (80%–100%) undergo trapping in α -6T but cannot be retransferred to C_{60} even at high fields and require long-range tunneling to neighboring donor sites. This slows down hole transport by 4–5 orders of magnitude in time, leading to a significantly reduced quasi-equilibrium hole mobility from $\mu_h = 0.4$ cm² V⁻¹ s⁻¹ in the C_{60} phase to $\mu_h = 6 \times 10^{-5}$ cm² V⁻¹ s⁻¹ for long-range tunneling between isolated donor sites (numbers at 10% dilution).

2.5. Relation between Phase Purity and Charge Motion

Figure 4a shows how the addition of α -6T disrupts the C_{60} phase. The increase in the electron energetic disorder of C_{60} has a clear onset at a donor fraction of 10% molar, in agreement with the transient data, where the temporal position of the electron extraction peak at the relevant (low) fields shifts to longer times at 25% molar (black dashed vertical line in Figure 2 is a guide to the eye). The increase in the energetic disorder is also reflected in the spectral blueshift of the EQE spectra at 2.5 eV, corresponding to an intermolecular^[21] absorption peak of C_{60} (Figure S8, Supporting Information). GIXD data shows that at $\approx 25\%$ –50% molar the diffraction rings corresponding to polycrystalline C_{60} are no longer observed^[23]—indicating amorphous C_{60} , for which the electron energetic disorder seems to saturate at $\sigma \approx 95$ meV (Figure 4a).

Figure 4b shows how donor–acceptor mixing affects the photogenerated electron mobility. The addition of the donor below 10% molar does not hinder electron transport in the C_{60} phase significantly—a quasi-equilibrium (long time) electron mobility of the order of $\mu_e = 1$ –2 cm² V⁻¹ s⁻¹ is retained, similar to that reported in neat C_{60} crystals.^[30] In contrast, at donor fractions higher than 10%, electron transport becomes increasingly dispersive with a time-dependent mobility due to carrier thermalization in the disorder-broadened density of states (DOS).^[39] The quasi-equilibrium electron mobility is then roughly an order of magnitude lower $\mu_e = 0.08$ cm² V⁻¹ s⁻¹ (at 25% molar) than at low donor content. Thus, at donor content below 10% molar the C_{60} phase can be considered as effectively pure for electron transport.

The hole energetic disorder in α -6T remains relatively constant around the mean $\sigma_h = 110$ meV, except for the 1.5% case. This is because hole transport at 5.7%–50% donor content is governed by hole trapping in isolated α -6T, followed by long-range tunneling through C_{60} to neighboring donor sites,

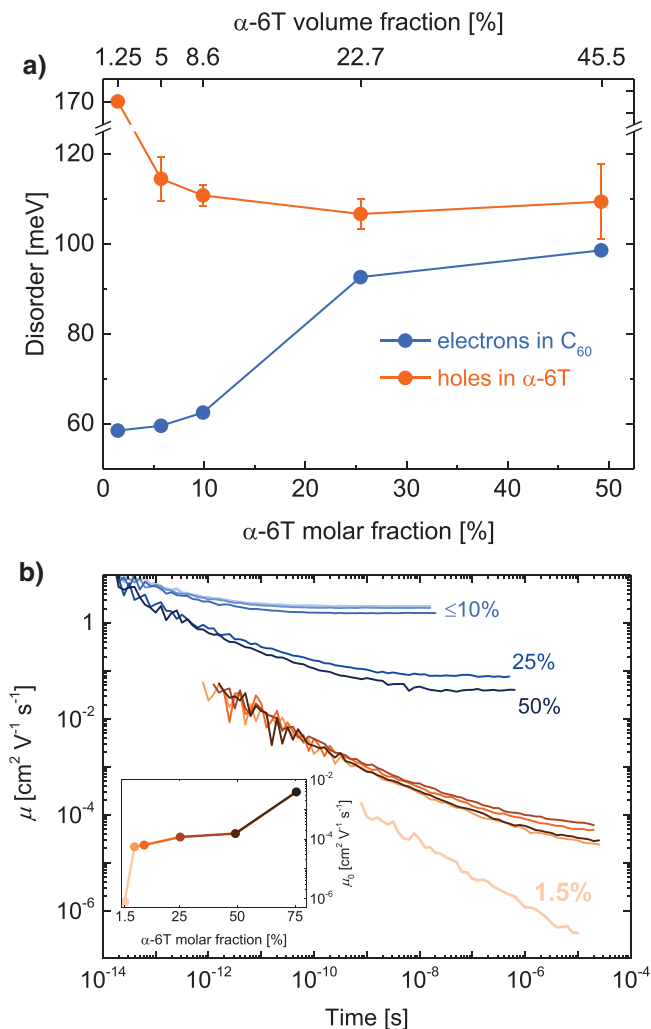


Figure 4. Energetic disorder and photogenerated carrier mobility with increasing α -6T content. a) Electron (blue symbols) and hole (orange symbols) energetic disorder of the Gaussian DOS versus α -6T content. Hole disorder was estimated both from transient and SCLC measurements, symbols indicate the mean, whereas errors bars indicate the corresponding standard error. b) Transient mobility of photogenerated holes (orange traces) and electrons (blue traces). The inset shows the experimental steady-state SCLC hole mobility μ_0 in the low carrier-density regime (see the Experimental Section), the increase in μ_0 at 1.5%–5.7% marks the onset for efficient long-range hole tunneling, whereas the increase at 50%–75% marks the formation of a continuous donor network.

whereas at 1.5% long-range tunneling is hindered. Thus, except for the 1.5% case, the resulting hole mobility kinetics are very similar and show only a slight increase with increasing donor content (Figure 4b), as corroborated by the lack of a significant temporal shift of the hole extraction peak in the transient extraction kinetics (black dashed vertical line in Figure 2). In this case the time-dependent hole mobility quantitatively describes the gradual relaxation of the hole population into low-lying α -6T sites.

The observed trends in the transient hole mobility and hole energetic disorder of α -6T are further experimentally confirmed by steady-state SCLC hole-only mobility measurements. The

inset of Figure 4b shows that the steady-state SCLC hole mobility μ_0 (in the low-concentration regime, see the Experimental Section) increases substantially at donor content higher than 1.5%, which marks the onset for efficient long-range hole tunneling. Following this onset hole mobility effectively plateaus—increases only slightly as the tunneling distance decreases with increasing donor content ($\mu_h = 5\text{--}15 \times 10^{-5} \text{ cm}^2 \text{ V}^{-1} \text{ s}^{-1}$ at 5.7%–50% molar).

Since at low donor content we vary the distance r between isolated α -6T sites, the inset of Figure 4b allows us to estimate the hole localization length α^{-1} in the framework of eGDM as $\mu \propto r^2 \exp(-2\alpha r)$. We obtain a surprisingly large number $\alpha^{-1} = 1 \pm 0.1 \text{ nm}$ (see Figure S9 in the Supporting Information), whereas typically $\alpha^{-1} \approx 0.1 \text{ nm}$ is assumed,^[36,38] based on earlier data for trinitrofluorenone (TNF):poly-*n*-vinylcarbazole (PVK) ($\alpha^{-1} \approx 0.11 \text{ nm}$) by Gill^[40] and for P3HT and OC₁C₁₀-PPV ($\alpha^{-1} \approx 0.15 \text{ nm}$) by de Leeuw et al. in ref. [41] (full material name for OC₁C₁₀-PPV is given in the Experimental Section). For large α^{-1} the hole wavefunction extends a larger distance from the donor site, enabling long-range tunneling.

We also observe an ≈ 40 -fold increase in μ_0 when the donor concentration increases to 75%, possibly indicating the formation of a continuous donor network, eliminating the need for long-range tunneling. Although we were unable to perform transient measurements on samples with high donor loading due to their weak 2nd harmonic intensity, the SCLC data for the 75% donor case do indicate a considerable ($\approx 43\times$) increase in the hole attempt-to-hop frequency ν_h and a similar hole disorder as for the other donor fractions $\sigma_h \approx 105 \text{ meV}$, see Table S3 (Supporting Information). The higher attempt-to-hop frequency reflects a shorter hopping distance, possibly due to the formation of a continuous donor network (Note S3, Supporting Information), increasing the carrier mobility up to $\mu_0 = 4 \times 10^{-3} \text{ cm}^2 \text{ V}^{-1} \text{ s}^{-1}$. Field-effect mobilities of $\approx 10^{-2} \text{ cm}^2 \text{ V}^{-1} \text{ s}^{-1}$ were reported for polycrystalline α -6T.^[42] The hole-only SCLC data thus indicates a change in the dominant hole transport mechanism—from long-range hole tunneling at 50% donor to hole transport via a continuous donor network at 75% donor. Most importantly, the combined dataset clearly indicates that C₆₀ domains containing an intermediate donor concentration (5.7%–50% molar, corresponding to isolated donor sites and a discontinuous donor network with aggregates) enable reasonable hole transport ($\mu_h = 5\text{--}15 \times 10^{-5} \text{ cm}^2 \text{ V}^{-1} \text{ s}^{-1}$ at 5.7%–50% molar).

Since the results presented here are expected to be general, we propose that Figure 4 may be used as a reference to what occurs in the fullerene phase upon the presence of a small amount of material/molecule with a donating character. As the photogenerated carriers in BHJs are expected to traverse both neat and mixed donor–acceptor domains, a combination of the above kinetics would be representative of the full charge transport kinetics.

3. Discussion

To the best of our knowledge, our data is the first experimental demonstration of following the transient motion of charges photogenerated in the CT manifold in a complete OPV device.

In agreement with earlier reports using internal quantum efficiency (IQE) measurements,^[43] we also observe that such photogenerated charges are extracted efficiently.

Generally, excitation in the CT manifold is expected to produce free carriers in the lowest lying DOS states, with little to no “excess energy” for further thermalization, and thus a low transient mobility. Our results show that this is not the case—if the material is sufficiently disordered, even charges photogenerated in the CT manifold undergo further thermalization with a time-dependent mobility. This is clearly visible in Figure 4, where σ gradually increases when going from almost non-disordered C₆₀, then to disordered C₆₀ and then to the highly disordered α -6T, leading to an increasingly time-dependent carrier mobility. The associated increasingly dispersive nature of charge transport is also directly visible in the increasingly convex shape of the extraction plateaus in Figure 2.

The possible importance of ambipolar transport in the fullerene phase of organic BHJ solar cells has been previously highlighted by several groups,^[13,44,45] challenging the general notion that hole transport is strictly facilitated only by the donor, and electron transport only by the acceptor. In fact, high hole mobility in neat C₆₀ has been well known since the 1990s.^[30] Our results show that although C₆₀ enables efficient hole transport, the fraction of holes extracted via C₆₀ at relevant fields for OPV devices is effectively zero. This is due to facile hole capture by the donor during hole transport in C₆₀. Therefore, at least for the case of small-molecule-donor and neat fullerene (C₆₀ or C₇₀) OPV devices, hole extraction only via the fullerene phase may be ignored.

Our results highlight the significance of another charge transport mechanism—long-range hole tunneling through several C₆₀ molecules. The effect of long-range charge tunneling between isolated small-molecule sites is similar to that of tie-chains in conjugated polymers, which were suggested to be responsible for charge transport between domains of ordered polymer.^[46] Both long-range tunneling and tie-chains effectively act as bridges between “favorable” sites and may occur concurrently. We expect that the tunneling processes discussed here are also relevant to OPVs using polymeric donors and/or acceptors, but the respective concentrations that are needed in a mixed phase to enable ambipolar transport may be different from the present system.

The emissive layer in some state-of-the-art organic light-emitting diodes (OLEDs) also consists of a mixture of a small concentration (3%–10% molar) of guest molecules, typically a phosphorescent dye, embedded in a host matrix. Using *ab initio* modeling, Wenzel et al. have recently demonstrated that charge transport between distant sites in such host–guest systems is mediated via the coherent process of molecular superexchange.^[47] Possibly the long-range hole tunneling that we experimentally demonstrate here for OPVs may be also explained by the theoretical framework laid out in ref. [47], as suggested by its authors.

Our results not only show that a continuous interpenetrating donor–acceptor network is not strictly necessary but also redefine the meaning of the commonly used terms of “neat”, “pristine”, or “pure phase.” More concretely, we have shown that C₆₀ may be considered as effectively pure for electron transport only if the molar fraction of the donor does

not exceed 10%. From a hole transport perspective, the same material, containing 90% of C₆₀ in α -6T, would generally be regarded as “not pure at all.” However, even at such low amounts of isolated donor, the hole mobility may be as high as $\mu_h \approx 6 \times 10^{-5} \text{ cm}^2 \text{ V}^{-1} \text{ s}^{-1}$ (at 10% molar) and is increasing with donor content ($\mu_h \approx 1.1 \times 10^{-4} \text{ cm}^2 \text{ V}^{-1} \text{ s}^{-1}$ at 25% molar), which is comparable to that reported for some neat donor materials used in OPV devices in the past. Therefore, the common notion that a continuous donor network is strictly necessary for efficient OPV device operation is erroneous.

4. Conclusion

We have shown, under conditions relevant to OPV device operation, that even when the donor sites are highly diluted (5.7%–10% molar) and the donor phase is discontinuous, hole transport between isolated donor sites can nevertheless occur by long-range hole tunneling through several buckminsterfullerene molecules, over distances as large as 4 nm. Hole transport between isolated donor sites occurs with a reasonably high hole mobility ($\mu_h = 5\text{--}15 \times 10^{-5} \text{ cm}^2 \text{ V}^{-1} \text{ s}^{-1}$, depending on the concentration of the donor). At low donor amounts (<10% molar) electron transport in the C₆₀ phase remains unperturbed ($\mu_e = 2 \text{ cm}^2 \text{ V}^{-1} \text{ s}^{-1}$) and the C₆₀ phase may be considered as effectively pure for electron transport. As such, C₆₀ domains containing only a trace amount of donor enable ambipolar transport by long-range hole tunneling—a continuous donor network is not strictly necessary for hole transport in organic solar cells.

Furthermore, we have shown that at high reverse bias and low donor concentration (1.5%–25% molar) a small fraction of the hole population (0%–20% of the total, depending on bias) can be transferred to and extracted via C₆₀ with a high hole mobility ($\mu_h = 0.1\text{--}2 \text{ cm}^2 \text{ V}^{-1} \text{ s}^{-1}$ for 25%–1.5% donor in C₆₀). Nevertheless, at field strengths relevant to OPV devices, facile hole capture by isolated donor sites rapidly reduces the fraction of holes transported in C₆₀ to zero. Subsequent hole motion occurs by long-range tunneling between isolated donor sites.

Since hole transport can occur via the acceptor phase, containing just a small fraction of material with a donating character, these results question the relevance of the commonly used terms of “neat”, “pristine”, or “pure phase” and whether a continuous interpenetrating donor–acceptor network is the ideal morphology of charge transport. The limits of long-range hole tunneling are yet to be explored.

5. Experimental Section

Full Material Names: poly(2-methoxy-5-(3',7'-dimethyloctyloxy)-*p*-phenylene vinylene) (OC₁C₁₀-PPV). Full names for other materials are given in the main text.

Device Fabrication: The photovoltaic devices were thermally evaporated at ultrahigh vacuum (base pressure <10⁻⁷ mbar) onto a glass substrate with a prestructured indium tin oxide (ITO) contact (Thin Film Devices, USA). 2 nm of MoO₃ were deposited to adjust the ITO work function and form an Ohmic hole contact. The active layer comprised 50 nm of C₆₀ (CreaPhys GmbH, Germany) blended with α -6T (Lumtec, TW) at α -6T molar fraction ranging from 1.5% to

75% (see Table S1 in the Supporting Information). Afterward, 8 nm of Bathophenanthroline (abcr GmbH, Germany), used as electron contact, was evaporated and finished with 100 nm of Al. The device was defined by the geometrical overlap of the bottom and the top contact with an active area of 1.68 mm². To avoid exposure to ambient conditions, the organic part of the device was covered by a small glass substrate, glued on top, providing encapsulation.

EQE Measurements: Measurements were performed using a xenon lamp (Oriel Xe Arch-lamp Apex, Newport, USA), a monochromator (Cornerstone 260 1/4m, Newport, USA), an optical chopper, and a lock-in amplifier (SR 7265, DPS Signal Recovery, USA). A silicon photodiode (Hamamatsu S1337, JP) was used as reference. This technique was used for the absolute determination of the EQE values.

Sensitive EQE Measurements: Monochromatic light with varying wavelengths were produced by illuminating a Newport Cornerstone 260 1/4m monochromator with chopped (140 Hz) white light of a quartz halogen lamp (50 W). The monochromatic light beam was focused onto the organic solar cell and its short-circuit current was amplified before it was analyzed with a lock-in amplifier (Signal Recovery 7280 DSP, Signal Recovery, Oak Ridge, USA). The time constant of the lock-in amplifier was chosen to be 1 s and the amplification of the preamplifier was increased to resolve the low photocurrents at low photon energies. The EQE spectrum was obtained by dividing the photocurrent of the solar cell by the flux of incoming photons, which was obtained with a calibrated silicon (Si) and indium–gallium–arsenide (InGaAs) photodiode.

Time-Resolved Measurements: Detailed description of the combined TREFISH and photocurrent experiment can be found in refs. [24,25]. Samples were pumped with 810 nm photons. Pump-fluences in the range of 25.4–87.4 μJ cm⁻² per pulse (1–3.56 × 10¹³ photons cm⁻² per pulse) were used, whereas for the 1.5% device a higher pump-fluence of 381 μJ cm⁻² per pulse (15.5 × 10¹³ photons cm⁻² per pulse) was necessary as the CT manifold of the 1.5% sample is rather weakly absorbing. Note that since CT absorption was orders of magnitude weaker than absorption of the constituent materials, the pump-fluences used in this study may be considered as relatively low. For the TREFISH experiment 810 nm probe photons were used. To obtain a reasonably good signal-to-noise ratio in the TREFISH experiment the probe-fluence was in the range of 299–314 μJ cm⁻² per pulse (12.2–12.8 × 10¹³ photons cm⁻² per pulse), whereas for the 1.5% device a higher probe-fluence of 564 μJ cm⁻² per pulse (23 × 10¹³ photons cm⁻² per pulse) was used. Due to limitations of the mechanical delay stage (3 ns max), the signal-to-noise ratio in the TREFISH experiment at longer time delays (>0.5–1 ns for the present devices) and RC limitations of electrical extraction (<20 ns) there is a lack of reliable data roughly in this range 1–20 ns. In cases where the photocurrent measurement is considered reliable below 20 ns, it is also shown, but is marked by thinner traces. Measurements at $U = 0$ V were not possible as the output resistance of the function generator (Tektronix AFG 3101) was found to change significantly. $U = -0.1$ V was used instead to ensure reliable measurements at (close to) short-circuit conditions.

Steady-State IV Measurements: IV characteristics were measured with a SMU (Keithley 2400, USA) at standard testing conditions (16 S-150 V.3 Solar Light Co., USA) with a mismatch corrected light intensity. For IV measurements at 785 nm illumination a continuous 1 mW laser was used.

Simulations: The most comprehensive description of the model can be found in ref. [37]. The Miller–Abrahams formalism was used to quantify with the least-number of unknown parameters the hopping rate of a charge carrier in a disorder-broadened Gaussian DOS. The real thickness of the BHJ layer was used in the simulations. Three charge carrier populations that could interact fully but were otherwise described by their own carrier hopping parameters were stimulated: the Gaussian energetic disorder σ and the attempt-to-hop frequency ν , which depends on the intersite distance, see Note S3 (Supporting Information). For each population the BHJ active layer was thus treated as an effective medium, meaning that local variations in the physical properties of the nanoscale morphology were not explicitly accounted for—obtained carrier hopping parameters represent “average” values over the entire

BHJ active layer. This minimizes the number of unknown simulation parameters to only those that are necessary to explain the experiments. A custom-made code was used to iteratively fit the experiments by least squares. The most important simulation parameters used/obtained from the model fits to transient and steady-state SCLC experiments are described in Table S3 (Supporting Information). All steady-state and transient mobilities were calculated for a fractional DOS occupancy of $c_0 = 10^{-4}$ at 300 K and an electric field strength of 0.5 V per 50 nm (1×10^5 V cm⁻¹).

Supporting Information

Supporting Information is available from the Wiley Online Library or from the author.

Acknowledgements

D.S., J.B., and K.V. were supported by the German Federal Ministry for Education and Research (BMBF) through the InnoProfile project “Organische p-i-n Bauelemente 2.2.” The work in Vilnius was supported by the Research Council of Lithuania (project MIP-85/2015). A.M. was supported by the Science Council of Sweden, and O.I. thanks the Knut and Alice Wallenberg foundation for instrumental funding and a Wallenberg Scholar grant.

Conflict of Interest

The authors declare no conflict of interest.

Keywords

charge carrier transport, fullerene domains, low donor concentration, organic photovoltaics, tunneling

Received: March 31, 2017

Revised: May 7, 2017

Published online: July 10, 2017

- [1] W. Zhao, D. Qian, S. Zhang, S. Li, O. Inganäs, F. Gao, J. Hou, *Adv. Mater.* **2016**, *28*, 4734.
- [2] J. Zhao, Y. Li, G. Yang, K. Jiang, H. Lin, H. Ade, W. Ma, H. Yan, *Nat. Energy* **2016**, *1*, 15027.
- [3] Y. Liu, J. Zhao, Z. Li, C. Mu, W. Ma, H. Hu, K. Jiang, H. Lin, H. Ade, H. Yan, *Nat. Commun.* **2014**, *5*, 5293.
- [4] F. C. Jamieson, E. B. Domingo, T. McCarthy-Ward, M. Heaney, N. Stingelin, J. R. Durrant, *Chem. Sci.* **2012**, *3*, 485.
- [5] S. Sweetnam, K. R. Graham, G. O. Ngongang Ndjawa, T. Heumüller, J. A. Bartelt, T. M. Burke, W. Li, W. You, A. Amassian, M. D. McGehee, *J. Am. Chem. Soc.* **2014**, *136*, 14078.
- [6] J. K. Gallaher, S. K. K. Prasad, M. A. Uddin, T. Kim, J. Y. Kim, H. Y. Woo, J. M. Hodgkiss, *Energy Environ. Sci.* **2015**, *8*, 2713.
- [7] A. C. Jakowetz, M. L. Böhm, A. Sadhanala, S. Huettner, A. Rao, R. H. Friend, *Nat. Mater.* **2017**, *16*, 551.
- [8] J. A. Bartelt, Z. M. Beiley, E. T. Hoke, W. R. Mateker, J. D. Douglas, B. A. Collins, J. R. Tumbleston, K. R. Graham, A. Amassian, H. Ade, J. M. J. Fréchet, M. F. Toney, M. D. McGehee, *Adv. Energy Mater.* **2013**, *3*, 364.
- [9] S. Mukherjee, C. M. Proctor, G. C. Bazan, T.-Q. Nguyen, H. Ade, *Adv. Energy Mater.* **2015**, *5*, 1500877.

- [10] S. Mukherjee, X. Jiao, H. Ade, *Adv. Energy Mater.* **2016**, *6*, 1600699.
- [11] C. M. Proctor, A. S. Kher, J. A. Love, Y. Huang, A. Sharenko, G. C. Bazan, T.-Q. Nguyen, *Adv. Energy Mater.* **2016**, *6*, 1502285.
- [12] S. Foster, F. Deledalle, A. Mitani, T. Kimura, K.-B. Kim, T. Okachi, T. Kirchartz, J. Oguma, K. Miyake, J. R. Durrant, S. Doi, J. Nelson, *Adv. Energy Mater.* **2014**, *4*, 1400311.
- [13] X. Guo, M. Zhang, J. Tan, S. Zhang, L. Huo, W. Hu, Y. Li, J. Hou, *Adv. Mater.* **2012**, *24*, 6536.
- [14] J. Huang, G. Li, Y. Yang, *Appl. Phys. Lett.* **2005**, *87*, 112105.
- [15] V. Pranculis, Y. Infahsaeng, Z. Tang, A. Devižis, D. A. Vithanage, C. S. Ponceca, O. Inganäs, A. P. Yartsev, V. Gulbinas, V. Sundström, *J. Am. Chem. Soc.* **2014**, *136*, 11331.
- [16] V. Abramavičius, D. A. Vithanage, A. Devižis, Y. Infahsaeng, A. Bruno, S. Foster, P. E. Keivanidis, D. Abramavičius, J. Nelson, A. Yartsev, V. Sundström, V. Gulbinas, *Phys. Chem. Chem. Phys.* **2014**, *16*, 2686.
- [17] M. Zhang, H. Wang, H. Tian, Y. Geng, C. W. Tang, *Adv. Mater.* **2011**, *23*, 4960.
- [18] K. Vandewal, J. Widmer, T. Heumueller, C. J. Brabec, M. D. McGehee, K. Leo, M. Riede, A. Salleo, *Adv. Mater.* **2014**, *26*, 3839.
- [19] Y. Zheng, W. J. Potscavage Jr., T. Komino, M. Hirade, J. Adachi, C. Adachi, *Appl. Phys. Lett.* **2013**, *102*, 143304.
- [20] Y. Zheng, W. J. Potscavage Jr., T. Komino, C. Adachi, *Appl. Phys. Lett.* **2013**, *102*, 153302.
- [21] S. Kazaoui, R. Ross, N. Minami, *Phys. Rev. B* **1995**, *52*, R11665.
- [22] K. Vandewal, K. Tvingstedt, A. Gadisa, O. Inganäs, J. V. Manca, *Phys. Rev. B* **2010**, *81*, 125204.
- [23] C. Lorch, K. Broch, V. Belova, G. Duva, A. Hinderhofer, A. Gerlach, M. Jankowski, F. Schreiber, *J. Appl. Crystallogr.* **2016**, *49*, 1266.
- [24] A. Devižis, A. Serbenta, K. Meerholz, D. Hertel, V. Gulbinas, *Phys. Rev. Lett.* **2009**, *103*, 027404.
- [25] A. Melianas, V. Pranculis, A. Devižis, V. Gulbinas, O. Inganäs, M. Kemerink, *Adv. Funct. Mater.* **2014**, *24*, 4507.
- [26] A. Melianas, V. Pranculis, Y. Xia, N. Felekidis, O. Inganäs, V. Gulbinas, M. Kemerink, *Adv. Energy Mater.* **2017**, *7*, 1602143.
- [27] J. Kniepert, I. Lange, N. J. van der Kaap, L. J. A. Koster, D. Neher, *Adv. Energy Mater.* **2014**, *4*, 1301401.
- [28] A. Foertig, J. Kniepert, M. Gluecker, T. Brenner, V. Dyakonov, D. Neher, C. Deibel, *Adv. Funct. Mater.* **2014**, *24*, 1306.
- [29] S. Albrecht, J. R. Tumbleston, S. Janietz, I. Dumsch, S. Allard, U. Scherf, H. Ade, D. Neher, *J. Phys. Chem. Lett.* **2014**, *5*, 1131.
- [30] E. Frankevich, Y. Maruyama, H. Ogata, *Chem. Phys. Lett.* **1993**, *214*, 39.
- [31] J. Sakai, T. Taima, K. Saito, *Org. Electron.* **2008**, *9*, 582.
- [32] R. H. Fowler, L. Nordheim, *Proc. R. Soc. London, Ser. A* **1928**, *119*, 173.
- [33] P. A. Lane, P. D. Cunningham, J. S. Melinger, O. Esenturk, E. J. Heilweil, *Nat. Commun.* **2015**, *6*, 7558.
- [34] J. M. Beebe, B. Kim, J. W. Gadzuk, C. Daniel Frisbie, J. G. Kushmerick, *Phys. Rev. Lett.* **2006**, *97*, 026801.
- [35] S. H. Choi, C. Risko, M. C. R. Delgado, B. Kim, J.-L. Brédas, C. D. Frisbie, *J. Am. Chem. Soc.* **2010**, *132*, 4358.
- [36] R. Coehoorn, W. F. Pasveer, P. A. Bobbert, M. A. J. Michels, *Phys. Rev. B* **2005**, *72*, 155206.
- [37] N. Felekidis, A. Melianas, M. Kemerink, *Phys. Rev. B* **2016**, *94*, 035205.
- [38] W. F. Pasveer, J. Cottaar, C. Tanase, R. Coehoorn, P. A. Bobbert, P. W. M. Blom, D. M. de Leeuw, M. A. J. Michels, *Phys. Rev. Lett.* **2005**, *94*, 206601.
- [39] A. Melianas, F. Etzold, T. J. Savenije, F. Laquai, O. Inganäs, M. Kemerink, *Nat. Commun.* **2015**, *6*, 8778.
- [40] W. D. Gill, *J. Appl. Phys.* **1972**, *43*, 5033.
- [41] C. Tanase, E. J. Meijer, P. W. M. Blom, D. M. de Leeuw, *Phys. Rev. Lett.* **2003**, *91*, 216601.
- [42] G. Horowitz, E. H. Mohsen, H. Riadh, *J. Appl. Phys.* **2000**, *87*, 4456.
- [43] K. Vandewal, S. Albrecht, E. T. Hoke, K. R. Graham, J. Widmer, J. D. Douglas, M. Schubert, W. R. Mateker, J. T. Bloking, G. F. Burkhard, A. Sellinger, J. M. J. Fréchet, A. Amassian, M. K. Riede, M. D. McGehee, D. Neher, A. Salleo, *Nat. Mater.* **2014**, *13*, 63.
- [44] S. M. Tuladhar, D. Poplavskyy, S. A. Choulis, J. R. Durrant, D. D. C. Bradley, J. Nelson, *Adv. Funct. Mater.* **2005**, *15*, 1171.
- [45] A. Gadisa, K. Tvingstedt, K. Vandewal, F. Zhang, J. V. Manca, O. Inganäs, *Adv. Mater.* **2010**, *22*, 1008.
- [46] R. Noriega, J. Rivnay, K. Vandewal, F. P. V. Koch, N. Stingelin, P. Smith, M. F. Toney, A. Salleo, *Nat. Mater.* **2013**, *12*, 1038.
- [47] F. Symalla, P. Friederich, A. Massé, V. Meded, R. Coehoorn, P. Bobbert, W. Wenzel, *Phys. Rev. Lett.* **2016**, *117*, 276803.